Int J Adv Manuf Technol (2018) 98:107–118
DOI 10.1007/s00170-017-0322-1

ORIGINAL ARTICLE

Swept surface-based approach to simulating surface topography in ball-end CNC milling

Jinting Xu[1] · **Hai Zhang**[1] · **Yuwen Sun**[2]

Received: 17 December 2016 / Accepted: 21 March 2017 / Published online: 18 May 2017

Abstract The parts, in automotive, aerospace, die/mold industry, which have extremely high demands on the quality and integrity of the surface, are usually milled by CNC machine tools. In order to obtain the desirable surface quality, it is an effective way to choose the appropriate cutting parameters before machining by simulating the surface topography formed in the milling process. To do so, this paper develops a model based on the swept surface of the cutting edge and *N*-buffer model for predicting the surface topography and studies the effect of various cutting parameters. In this developed model, the mathematical equation of the cutting edge is first given, and then based on the relative motion between the cutter and the workpiece, the swept surface of the cutting edge along the tool path is accurately analyzed and modeled from the perspective of kinematics, which is used to describe realistically the cutting interaction between the cutter and the workpiece. Subsequently, the milling process is simulated by an improved *N*-buffer model by means of the proposed accurate interpolation method for calculating the cusp height. This procedure presents the advantage of not requiring any numerical iteration or approximation to gain the cusp height of any point on workpiece. On basis of the model, the effect of the cutting parameters such as spindle speed, feedrate, inclination angle, path interval, and cutter runout is investigated. Finally, the real machining experiments are performed and compared with the predicted results. The simulated surface topography shows a good agreement with the experimental one. This demonstrates that the developed model can predict accurately the surface topography and also provide the great potential for the surface quality control and the cutting parameter selection in actual production.

Keywords Surface topography · Surface roughness · Ball-end machining · Swept surface · *N*-buffer model

✉ Jinting Xu
xujt@dlut.edu.cn

[1] School of Automotive Engineering, Dalian University of Technology, Dalian 116024, People's Republic of China

[2] School of Mechanical Engineering, Dalian University of Technology, Dalian 116024, People's Republic of China

1 Introduction

Ball-end milling is one of the most widely applied metal removal processes in automotive, aerospace, and die/mold industry and the machined surface are largely used to mate with other parts to obtain certain functions such as kinetic design and machinery behavior [1]; thus, the surface quality, which is determined by the micro surface topography, has great influence on mechanical properties of the parts, such as wear, tensile, fatigue, corrosion, and lubrication. As the surface topography is mainly dependent on the cutting parameters, tool geometry, etc., to obtain such a fairly qualified surface, the appropriate cutting parameters have to be carefully selected [2]. So far, in the most of workshops, the machine operators select the cutting parameters either by conducting "trial and error" experiments or according to the previous work experiences or any machining data hand books [3]. Such traditional selection of cutting parameters is non-technical, and time and cost are unnecessarily wasted. For this purpose, it is necessary to develop an accurate model to predict the machined surface topography before machining in order to achieve the desirable surface finish with the proper cutting parameters. In the following, some background and past works on the prediction of the surface topography will be first reviewed.

1.1 Related works

In practice, there are two types of commonly used ball-end mills, i.e., ball-end mills with helix and straight flutes, as shown in Fig. 1a, b. Initially, for the convenience of calculating the path interval cusp between two adjacent tool paths, the ball-end mill is modeled by a spherical-tool approximation model, i.e. a solid of revolution, while only the translation of the mill along the tool path is considered and the cutting action of the individual flute is ignored [4, 5]. Based on the simplification, most CAD/CAM systems, such as Unigraphic/NX, CATIA, and MasterCAM, have already provided good simulating procedures to view path interval cusp geometry over the whole surface, which is a series of hemispherical grooves across the machined surface. But this method is aiming to estimate the path interval cusp and unable to generate the real surface topography on the part because of ignoring the influence of the individual mill flute on the material removal process. As improvement, Kim and Chu [6] considered the rotation motion of the cutting edge and simplified its complicated trochoid path to circular path along the tool path, so that the topography of the machined surface is estimated by the superposition of the semispherical or ellipsoidal textures which are separated by the feed per tooth, and the analytical formulas for the feed-cusp height are also given. Based on the model, the effects of the mill mark and runout are studied on the surface topography. Later, Ryu et al. [7] extended this texture superposition approach to face milling of the flat-end mill, considering the back cutting. With the consideration of the of the actual trochoid path of cutting edge, Jung et al. [8, 9] developed a so-called ridge method to simulate the surface topography, in which the analytical equation of three types of ridges is derived based on the disk-tool approximation model in which the helix angles of the flutes are negligible when cutting using the ball-end mill with helix flute in Fig. 1a. This method

(a) (b)

Fig. 1 Two commonly used ball-end mills. **a** Ball-end mill with helix flutes. **b** Ball-end mill with straight flutes

is very efficient in the term of calculation; however, as pointed out by them, it is only carried out for the plane cutting mode and is limited to be extended to the sculptured surface machining.

In order to be applied to the complex surface machining, numerical simulation based on *Z*-map or *N*-buffer model is usually adopted, instead of analytical calculation, for predicting the surface topography. But, in most of methods, the cutting edge has been still approximated simply by a semicircular arc [10–12] and elliptical curve [13], or discretized into micro-elements slice by slice along the cutter axis and every micro-element is represented by one point or line segment in order to take into account conveniently tool wear, deflection, vibration [14–17]. When simulating the cutting process, Liu et al. [10] proposed the concept of the cutting motion discretization. At every discretized motion position, the interaction of the cutting edge and *Z*-map model of the workpiece is used to represent the surface topography. In [11], the workpiece surface is sampled on XY plane and at each sample point a reference spike with a specified initial height is set, then the surface topography is represented by the altitudes of the spikes that are determined by the heights of the remainders after being cut using the cutting edge. Similar work can be also found in [12]. It is noted, in these above methods, that the cutting edge motion is discretized according to the time, but the workpiece surface to the u-v parameters. Often, this difference leads to that the cutting edges may not intersect really the reference lines of *Z*-map so that some points, which should be swept by the cutting edges, might be missed at certain calculation positions. So, a tolerance has to be adopted to solve the limitation in the simulation. Buj-Corral et al. [13] discretized the workpiece into a series of horizontal plane along *Z* direction and each plane is discretized again according to a square matrix whose points are separated by a specified distance. Then, the surface topography is simulated by intersecting this discretizing model of the workpiece with the elliptical curve that approximates the cutting edge. But, as mentioned by them, unless the workpiece discretization is proper, the error produced by this method cannot be neglected. In [14–16], the motion equation of the discrete point of the cutting edge is first accurately modeled, and then the intersections of the paths of all these discrete points with the parallel reference planes are connected into the surface topography. The intersection is usually determined by the numerical iterations such as Newton-Raphson method. Recently, in the work of Arizmendi et al. [17], the trajectories of the discrete points of the cutting edge are cut by the planes perpendicular to the feed direction obtaining a set of transcendental equations that are solved by transforming them to polynomial equations through Chebyshev expansions, avoiding the requirement of any starting point to achieve the solution.

Actually, the mechanism behind the formation of the topography of the surface is very dynamic and complicated, and

process dependent. To predict the surface topography more realistically, the model and motion of the cutting edge must be described accurately, and the simulation of the cutting action of the cutter must be also as close to the real material removal process as possible [18]. Zhang et al. [19] described the motion of the cutting edge with a helix angle and proposed a general numerical method to determine the parameters of cutting edge at any point of workpiece, thereby obtaining the cusp height of the point. Mathematically, it is similar to solving the intersection point of the cutting edge and the reference line at the point. In the latest works [20–22], Quinsat et al. also modeled the real motion of the cutting edge, but in the cutting simulation, they discretized the motion of the cutting edge on the time t. At each t, the intersection of the cutting edge and the reference plane is calculated. For the same discretized position of the surface, the lowest altitude is used to represent the final remainder of cutting. Actually, In simulating of the cutting processes, the intersection of the cutting edge with the reference lines or the reference planes is very complicated, because at the same position, the intersections may be up to three [23]. If considering the cutting in the adjacent tool path, up to six intersections occur possibly. It may lead to great confusion of selecting the initial point to achieve the proper solution.

1.2 Motivation of this paper

From the view of kinematics, when the ball-end milling proceeds along a tool path, the material will be continuously removed by the swept surfaces of the cutting edges [18, 24]. Due to the trochoid path of the cutting edge in the cutting processes, the same position on the workpiece may be swept three times, and at a latter time, the remained material after cutting by this cutting edge will be swept again by the next cutting edge. Further, the material left on the workpiece after milling along the current tool path will be cut again by the swept surfaces of the cutting edges along the adjacent tool path. So, the cutting edge and its swept surface along the tool path have to be modeled accurately for the topography prediction of the surface. In this way, other factors such as tool runout, wear, deflection, and vibration can be combined conveniently into this model of the swept surface, and study deeply the effect of these parameters. In addition, the simulation of the material removal process of the swept surface cannot only avoid the tolerance resulted from the difference between the discretizing parameters of the cutting motion and the workpiece, but also overcome the confusion on calculation of the remained material height in the numerical methods. For the purposes, this paper develops a swept surface based method for simulating the surface topography and the details will be discussed next.

2 Model of cutting edge

In the section, different from existing methods, the univariate (z) equation of the cutting edge is derived which is very critical for the following swept surface modeling and cutting simulation. Figure 2 shows the geometry of the rotary cutter which is modeled mathematically by:

$$\Sigma : \boldsymbol{r}_{\text{cutter}}(z,\varphi) = [r(z)\cos\varphi, r(z)\sin\varphi, z]^{\mathrm{T}} \tag{1}$$

where φ is the rotation angle, $r(z)$ is the turning radius of arbitrary point on the rotary surface and z is the axial distance from $\boldsymbol{O}_T$ which is the center of the ball-end cutter, and $z \in [0, -R]$, $\varphi \in [0, 2\pi]$. To obtain the model of the cutting edge, it has to reduce the number of free variables in Eq. (1). If z is selected as the variable of the equation of the cutting edge, φ can be represented by

$$\varphi_j(z) = \frac{2(j-1)\pi}{N} + \gamma(z) \tag{2}$$

where j denotes the jth cutting edge, N is the number of the cutting edge, $\gamma(z)$is the location angle between $\boldsymbol{O}_{\mathrm{T}}\boldsymbol{P}_t$ and $\boldsymbol{O}_{\mathrm{T}}\boldsymbol{P}_0$, which is the key parameter of the cutting edge. As shown in Fig. 3, $\boldsymbol{P}_t$ is the projection on plane $\mathrm{X_T}-\mathrm{Y_T}$ of point $\boldsymbol{P}$ on the cutting edge, and $\boldsymbol{P}_0$ is the intersection of the cutting edge and plane $\mathrm{X_T}-\mathrm{Y_T}$, which can be seen as the starting point of the cutting edge in this paper.

It is well known that there are two kinds of helix cutting edges, i.e., the equal-lead and helix angle. Here, the used in this paper is equal-helix angle mill which is a common cutter used widely in the milling process. It must satisfy the following equation (Eq. (3)) on the rotary profile

$$\tan\theta = \frac{r(z)d\gamma(z)}{\sqrt{dr(z)^2 + (dz)^2}} \tag{3}$$

where parameter θ is the helix angle for the cutting edge. When using the ball-end cutter, according to the geometric

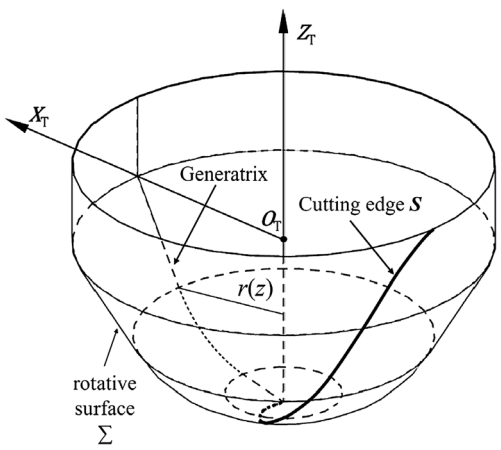

Fig. 2 General geometry of the rotary cutter

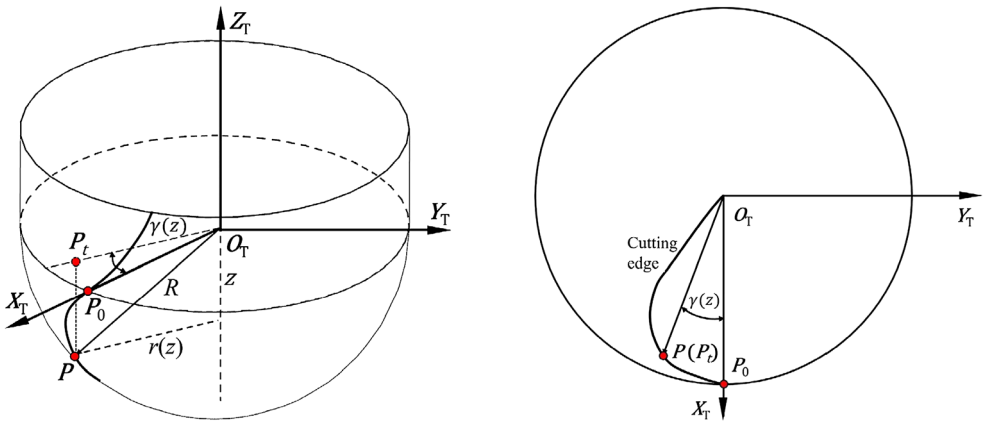

Fig. 3 Geometry of the ball-end cutter with equal-helix angle

relationship shown in Fig. 3, $r(z)$, at the hemispherical part of the cutter which is also the focus of interest can be computed by the equation,$r(z) = \sqrt{R^2-z^2}$. Then, putting $r(z)$ into Eq. (3) can obtain the parameter $\gamma(z)$:

$$\gamma(z) = \frac{1}{2}\tan\theta ln\left(\frac{R+z}{R-z}\right), \quad z < R \tag{4}$$

Then, putting $r(z)$ and $\gamma(z)$ into Eq. (1) and (2), the expression $\boldsymbol{S}(z)$, which stands for the cutting edge, is gained.

3 Swept surface of cutting edge

3.1 Coordinate systems in five-axis ball-end milling

To accurately model the swept surface of the cutting edge, the coordinate systems involved in five-axis ball-end milling is established first as follows.

(1) Cutter coordinate system (CCS), $\{\boldsymbol{O}_T; \boldsymbol{X}_T, \boldsymbol{Y}_T, \boldsymbol{Z}_T\}$. A local coordinate system attached to the cutter where $\boldsymbol{Z}_T$ is along the cutter axis direction. Initially, $\boldsymbol{X}_T$ and $\boldsymbol{Y}_T$ are consistent respectively with $\boldsymbol{X}_w$ and $\boldsymbol{Y}_w$ of the workpiece coordinate system;
(2) Spindle coordinate system (SCS), $\{\boldsymbol{O}_S; \boldsymbol{X}_S, \boldsymbol{Y}_S, \boldsymbol{Z}_S\}$. A local coordinate system fixed on the spindle of the machine tools. $\boldsymbol{Z}_S$ is along the spindle direction and parallel to the cutter axis, and in SCS the cutter revolves around the spindle with angle speed ω, as shown in Fig. 4;
(3) Cutter contact coordinate system (GCS), $\{\boldsymbol{O}_G; \boldsymbol{X}_G, \boldsymbol{Y}_G, \boldsymbol{Z}_G\}$. As shown in Fig. 5. The origin of GCS is cutter contact (CC) point on the tool path, $\boldsymbol{X}_G$ axis points to the path interval direction, $\boldsymbol{Y}_G$ axis is along the feed direction and $\boldsymbol{Z}_G$ axis is the normal direction of workpiece surface at CC point;
(4) Workpiece coordinate system (WCS), $\{\boldsymbol{O}_w; \boldsymbol{X}_w, \boldsymbol{Y}_w, \boldsymbol{Z}_w\}$. A global coordinate system, in which the workpiece surface, the tool path and the topography of the machined surface are described and modeled.

3.2 Rotary profile of cutting edge considering runout

Theoretically, in addition to the tool geometry and cutting condition, other factors, such as cutter runout, wear, and deflection, can be also combined in modeling of the swept surface as long as their equations with respective to z or t is established. In this way, the effect of these parameters can be studied. In the milling experiments, if a very stable machining center, new cuter and small depth of cut are used and the flooding coolant is supplied, the influence on the surface topography of the vibration, deflection, and wear of the cutter and even the change of temperature can be suppressed effectively. But, the cutter runout in the milling process is almost inevitable due to the existence of manufacturing and installation errors of the cutter. Thus, in the paper, the cutter runout will be taken into consideration in modeling of the swept surfaces, and for the convenience of the discussion, only the parallel-axis runout is studied. In Fig. 4, $\boldsymbol{O}_S\boldsymbol{O}_T$ denotes the parallel-axis runout, which is represented by the initial angle ε and the distance e between $\boldsymbol{O}_S$ and $\boldsymbol{O}_T$. Under this situation, the transformation matrix $\boldsymbol{M}_{C\to S}$ from CCS to SCS can be formulated as

$$\boldsymbol{M}_{C\to S} = \begin{bmatrix} \cos(\omega t) & -\sin(\omega t) & 0 & 0 \\ \sin(\omega t) & \cos(\omega t) & 0 & 0 \\ 0 & 0 & 1 & 0 \\ 0 & 0 & 0 & 1 \end{bmatrix} \begin{bmatrix} 1 & 0 & 0 & e\cos\varepsilon \\ 0 & 1 & 0 & e\sin\varepsilon \\ 0 & 0 & 1 & 0 \\ 0 & 0 & 0 & 1 \end{bmatrix} \tag{5}$$

where t is the machining time along the tool path. In SCS, the rotary profile of the cutting edge considering the cutter runout about the spindle is represented by

$$\boldsymbol{S}^{(\mathrm{scs})}(z) = \boldsymbol{M}_{C\to S}\boldsymbol{S}(z) \tag{6}$$

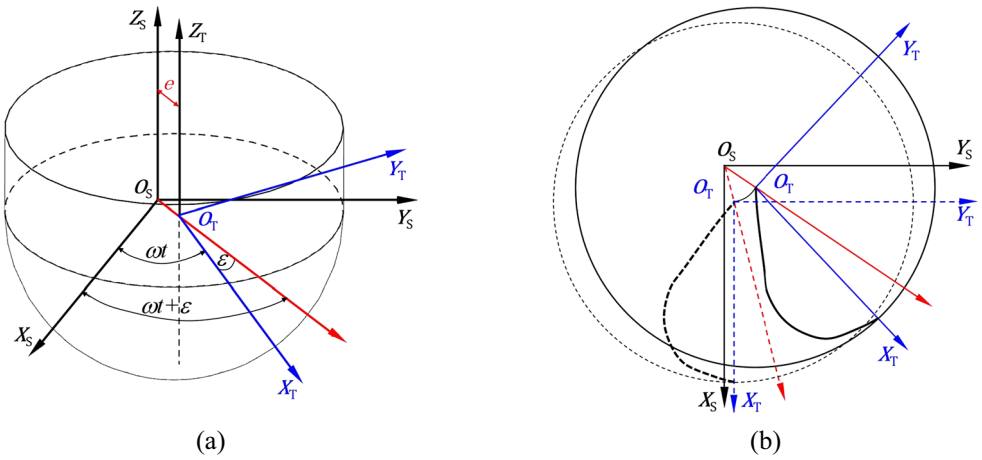

Fig. 4 **a** Geometry of the ball-end mill with parallel-axis runout. **b** Top view of parallel-axis runout

On basis of Eq. (6), the rotary profile in GCS at each CC point can be obtained by means of the transformation from SCS to GCS, $\boldsymbol{M}_{S\to G}$, which is the product of two rotation matrix. One is the rotation of the spindle about $\boldsymbol{X}_G$ axis, the other is one of the spindle around $\boldsymbol{Z}_G$ axis. $\boldsymbol{M}_{S\to G}$ is represented mathematically by

$$\boldsymbol{M}_{S\to G}=\begin{bmatrix}\cos\beta & -\sin\beta & 0 & 0\\ \sin\beta & \cos\beta & 0 & 0\\ 0 & 0 & 1 & 0\\ 0 & 0 & 0 & 1\end{bmatrix}\begin{bmatrix}1 & 0 & 0 & 0\\ 0 & \cos\alpha & -\sin\alpha & 0\\ 0 & \sin\alpha & \cos\alpha & 0\\ 0 & 0 & 0 & 1\end{bmatrix} \tag{7}$$

where α, β are the tilt angle and the yaw angle of the tool orientation in LCS, respectively, as shown in Fig. 6. According to Eq. (7), the rotary profile of the cutting edge in the local GCS can be modeled by

$$\boldsymbol{S}^{(\mathrm{gcs})}(z)=\boldsymbol{M}_{S\to G}\boldsymbol{M}_{C\to S}\boldsymbol{S}(z) \tag{8}$$

3.3 Swept surface of cutting edge in WCS

Typically, in the milling process, the feed direction is always constantly changing; thus, the directions of three axes of GCS are not usually consistent with that of WCS unless in the case of linearly feeding on $X_w - Y_w$ plane. Thus, to obtain the swept surface of the cutting edge along the tool path in WCS, the transformation from GCS to WCS has to be applied to $\boldsymbol{S}^{(\mathrm{gcs})}(z)$, which can be written as

$$\boldsymbol{M}_{G\to W}=\begin{bmatrix}\boldsymbol{X}_G & \boldsymbol{Y}_G & \boldsymbol{Z}_G & 0\\ 0 & 0 & 0 & 1\end{bmatrix}^{\mathrm{T}}\begin{bmatrix}\boldsymbol{E}_{3\times3} & \boldsymbol{a}(t)\\ 0\,0\,0 & 1\end{bmatrix} \tag{9}$$

where $\boldsymbol{a}(t)$ is the vector from the origin of WCS to that of GCS at time t, as shown in Fig. 5, and $\boldsymbol{E}_{3\times3}$ is a 3 × 3 identity matrix. By means of Eq. (8) and (9), the swept surface, $\boldsymbol{\Psi}(z, t)$, which is formed by the cutting edge proceeding along tool path with feedrate f and simultaneously rotating with angle speed ω in the milling process, can be modeled by the following equation,

$$\boldsymbol{\Psi}(z,t)=\boldsymbol{M}_{G\to W}\boldsymbol{M}_{S\to G}\boldsymbol{M}_{C\to S}\boldsymbol{S}(z) \tag{10}$$

Figure 7 gives an example of the swept surfaces formed by one cutting edge along two adjacent tool paths. It is seen that the intersections of the swept surface itself and between neighboring swept surfaces are very complex. This also verifies that, as mentioned early, the same position on the workpiece may be cut repeatedly by the swept surfaces. It is very disadvantageous for those numerical iteration methods, which are used to calculate the intersection points of the reference line or plane with the cutting edge, due their dependency on the good starting point.

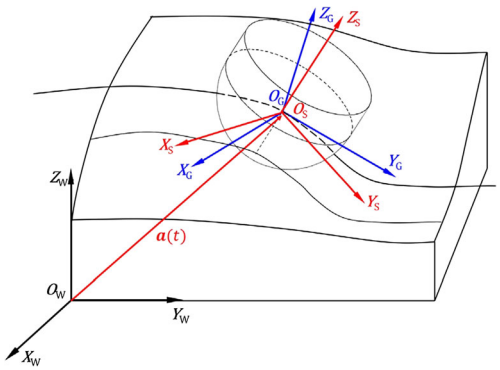

Fig. 5 Transformation between GCS and WCS

4 Simulation of surface topography

The simulation of the material removal process relies on the well-known *N*-buffer model, in which the workpiece surface is discretized by the lines directed along the normal to the surface and the cutter is represented by the produced swept surface. This discretized surface model is then truncated by the swept surfaces along the tool path, and the remained part

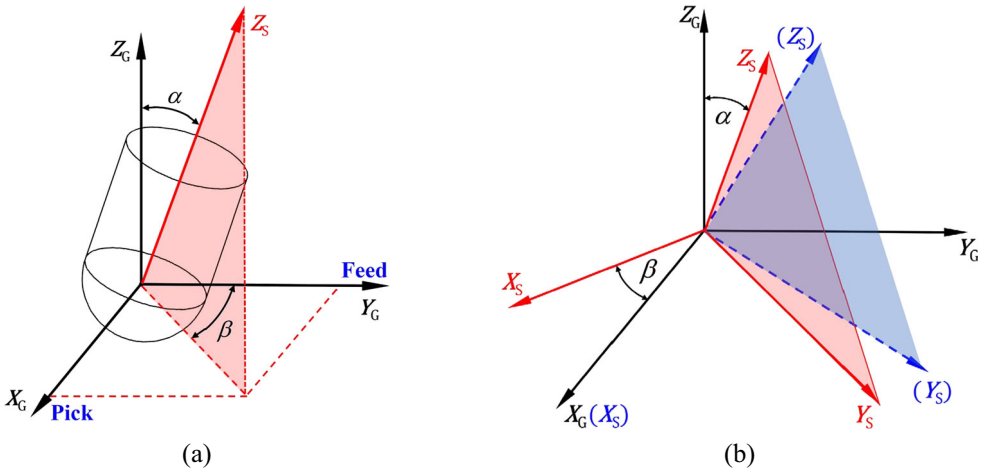

Fig. 6 **a** Tool orientation and **b** transformation

defines the surface topography. The emphasis of this section focuses on calculation of the intersection of the reference line with the swept surfaces.

4.1 N-buffer model of workpiece surface

Assume that the workpiece surface is a parametric surface described by $\boldsymbol{s}(u, v)$, the surface is first meshed into a grid. The meshing point $(\boldsymbol{s}_{a,b}, h_{a,b})$ is determined by

$$\boldsymbol{s}_{a,b} = \boldsymbol{s}(a\Delta u, b\Delta v), a = 0, 1, \cdots, n; b = 0, 1, \cdots, m \qquad (11)$$

where Δu and Δv are mesh sizes in the u and v directions on the parameter plane, which are chosen according to the requirement for the accuracy and computation time. Generally, the distance between two adjacent mesh points should be not more than 2 μm. $h_{a,b}$ records the height of remainder after each cutting, and initially it is equal to the depth of cut specified by the users. At each meshing point, the reference line is defined as follows:

$$\text{Line}: \quad \boldsymbol{L}_{a,b} = \boldsymbol{s}_{a,b} + h_{a,b}\boldsymbol{n}_{a,b} \qquad (12)$$

In Eq. (16), $\boldsymbol{n}_{a,b}$is the unit normal vector of the workpiece surface at the meshing point $\boldsymbol{s}_{a,b}$. Figure 8 shows a discretized workpiece surface model.

4.2 Discretization of the swept surface

Due to the nonlinearity of the equation of swept surface and its multi-intersections with the reference line, it is not an easy task to gain the remaining height of the reference lines using the numerical iteration methods depending on good starting point. In order to calculate the intersection of the swept surface with the reference line, an interpolation method is proposed. For the implementation of the method, the swept surface needs to be meshed into a rectangle grid and the meshing point is determined by

$$\boldsymbol{\Psi}_{i,j} = \boldsymbol{\Psi}(i\Delta z, j\Delta t), i = 0, 1, \cdots, n_z; j = 0, 1, \cdots, m_t \qquad (13)$$

where Δz and Δt are mesh sizes in the z and t directions. Generally, the gird of the swept surface does not need to be very dense for saving the computation time because the cusp

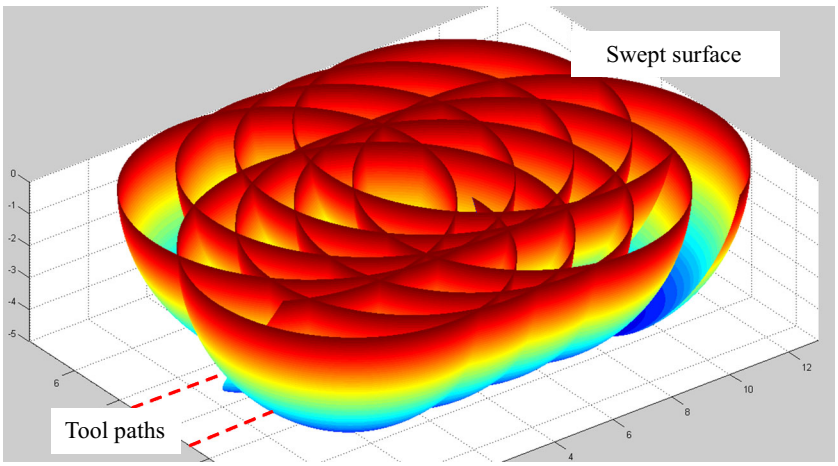

Fig. 7 Swept surfaces of one cutting edge along two adjacent tool paths

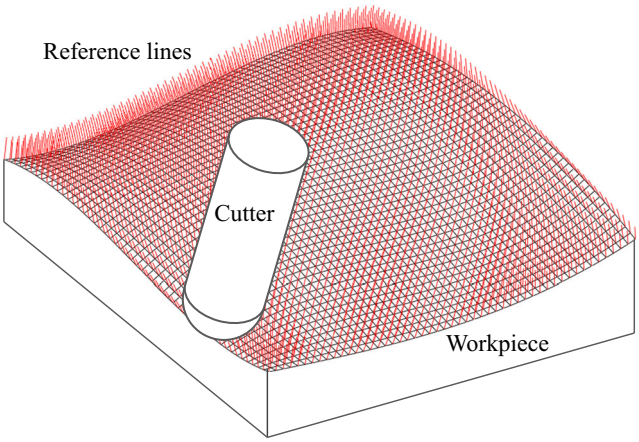

Fig. 8 *N*-buffer model of workpiece surface

point on the swept surface is not the grid point, but the one interpolated from four grid points. According to our experiment, Δz is in the range of $0.05-0.1$mm and Δt in $(0.005-0.001)/n$ can generally produce a desired result, where n is the spindle speed. In meshing the swept surface, the topological relations among the meshing point, edge, and facet need also to be created at the same time, so that, for a known meshing point, its neighboring edges and rectangle facets can be found quickly. It is very important to implement efficiently the proposed interpolation method for calculating the cusp point.

4.3 Determination of cutting region

For *N*-buffer model, the main challenger is its computation efficiency. A naive implement of calculating the cusp height is to attempt to intersect all the reference lines with the swept surface, but it will become very costly. Here, to avoid a great number of attempted intersections, the cutting region that contributes to the final surface topography is first roughly determined. Actually, the surface topography consists of the path-interval and feed-interval scallops which are separated by the path interval, w_p, and the feed per tooth, f_z, respectively, as shown in Fig. 9. According to this information, the cutting region, proceeding every distance of f_z along the tool path, is simplified to a circular region which radius is R_{cr},

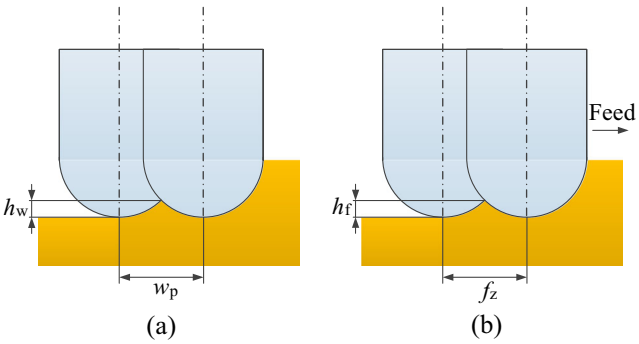

Fig. 9 **a** The path-interval scallop and **b** the feed-interval scallop of the ball-end cutter

$$R_{cr} = \max\{f_z, w_p\} \tag{14}$$

For the implementation of the proposed method, only the reference lines in the cutting region are attempted to intersect with the swept surface. Compared with the number of all reference lines, the number of the reference lines in the cutting region is small so that the efficiency of the simulating algorithm can be improved.

4.4 Intersection of reference line with swept surface

As shown in Fig. 10, meshing point, $\boldsymbol{s}_{a,b}$, of the workpiece surface is taken as example to discuss the calculation of cusp height at this point. First, it is needed to find the closest point of $\boldsymbol{s}_{a,b}$ from all meshing point $\{\boldsymbol{\Psi}_{i,j}\}$ along the reference line. This can be easily implemented by the graphics algorithms [25]. Once the closest point of $\boldsymbol{s}_{a,b}$ is found, as shown in Fig. 10b, assume that the closest point is $\boldsymbol{\Psi}_{i,j}$, the neighbor rectangle facets of $\boldsymbol{\Psi}_{i,j}$is searched to find the intersection of the reference line $\boldsymbol{L}_{a,b}$ and the facet. Assume that the intersection is $\boldsymbol{P}_L^{'}$ that should meet the following condition of

$$\sum \text{Area\_tri}\left(\boldsymbol{\Psi}_{i,j}\right) = \text{Area\_rect}\left(\boldsymbol{\Psi}_{i,j}\right) \tag{15}$$

where the left stands for area sum of four triangles which are formed by the intersection $\boldsymbol{P}_L^{'}$ and the four corner points of the rectangle, as shown in Fig. 10b, and the right is the area of the rectangle. In meshing the swept surface, the parameters of the meshing points have been also stored, so that the parameters of $\boldsymbol{P}_L^{'}$ can be calculated by weighted sum of the parameters of four corners of the rectangle with weights proportional to the distances of $\boldsymbol{P}_L^{'}$ and four corners. The parameter (z_L, t_L) of $\boldsymbol{P}_L^{'}$ is calculated by

$$\begin{cases} (z_L, t_L) = \sum\limits_{\substack{e=i,i-1 \\ f=j,j+1}} w_{e,f}\left(z_{e,f}, t_{e,f}\right) \\ w_{e,f} = \text{dist}\left(\boldsymbol{P}_L^{'}, \boldsymbol{\Psi}_{e,f}\right) \Big/ \sum\limits_{\substack{e=i,i-1 \\ f=j,j+1}} \text{dist}\left(\boldsymbol{P}_L^{'}, \boldsymbol{\Psi}_{e,f}\right) \end{cases} \tag{16}$$

where dist(·) stands for the distance of two points. Once the parameters (z_L, t_L) is obtained using Eq. (16), which is then put into Eq. (10) to calculate the accurate intersection of the reference line and the swept surface. The height of cutting cusp can be determined by.

$$h_{a,b} = \text{dist}\left(\boldsymbol{s}_{a,b}, \boldsymbol{\Psi}(z_L, t_L)\right) \tag{17}$$

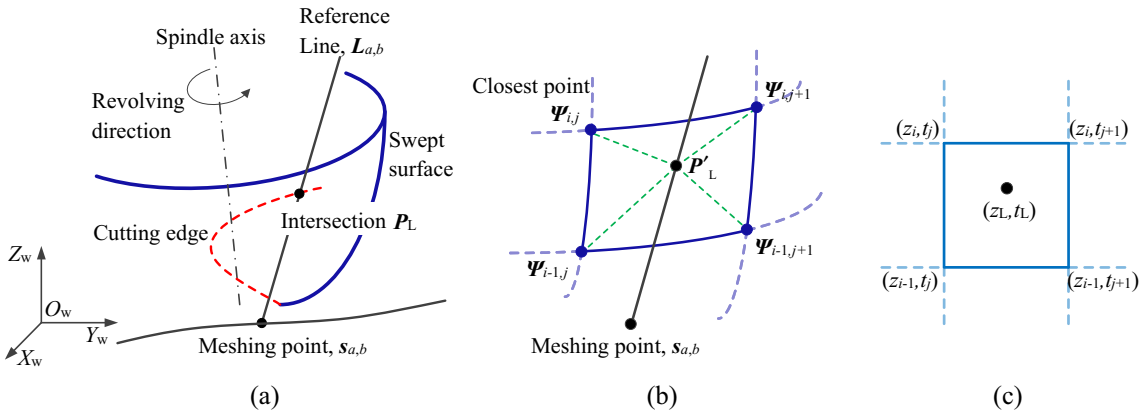

Fig. 10 Calculation of the intersection of the reference line and the swept surface. **a** Reference line and swept surface. **b** Intersection of the reference line and the rectangular plane. **c** The parameter point of the intersection on the z-t parameter plane

The remaining parts of the reference lines are used to define the surface topography.

5 Simulation and experiment verifications

5.1 Experiment set-up

The algorithms involved in this paper are coded in C++ language and implemented on a PC with an Intel 3.4 GHZ and 8.0G physical memory. On basis of this, a series of simulating and milling experiments are carried out to verify the proposed predicting model for the surface topography. A Deckel Maho DMU50 5-axis CNC machine center with a maximum spindle speed of 18,000 rmp is used for the real milling experiments, as shown in Fig. 11. The workpiece material is AL-2024. A 2-flute carbide ball-end cutter with a helix angle of 45° and a diameter of 10 mm is used. The surface topography, profile, and roughness of the machined surface are measured by an interferometer, Zygo New View 5000, shown in Fig. 12. The arithmetic mean roughness Ra is adopted to describe the surface roughness due to its wide application in engineering, and a sampling length of 2.5 mm is applied in surface inspection. To reduce the measurement error as much as possible, Ra is averaged over three separated measurements whose measuring points are uniformly distributed on the milled surface.

Though there are many cutting parameters which affect the surface topography, the selected cutting parameters for this study are feed per tooth, tool orientation, path interval, and cutter runout, since these parameters have the greatest effect on the success of the milling operations [1, 3]. More importantly, these parameters can be easily changed in the milling process, except cutter runout, without the need of additional device and time. Thus, in this study, only these parameters are considered. In addition, to reduce the effect of other factors as much as possible, the new cutter, small depth of cut, and flooding coolant are applied in the actual cutting experiment. The selected cutting parameters for the study are listed in Table 1. According to our experiments, when the cutter runout is set 10 μm, the simulating surface topography and roughness have a good agreement with the experimental ones, so when studying the effect of feed per tooth, tool orientation and path interval, e is set 10 μm, and other values of the runout in the table are used to study the effect of the cutter runout by simulation in Section 5.5.

Fig. 11 DMU 50 five-axis CNC machine tool

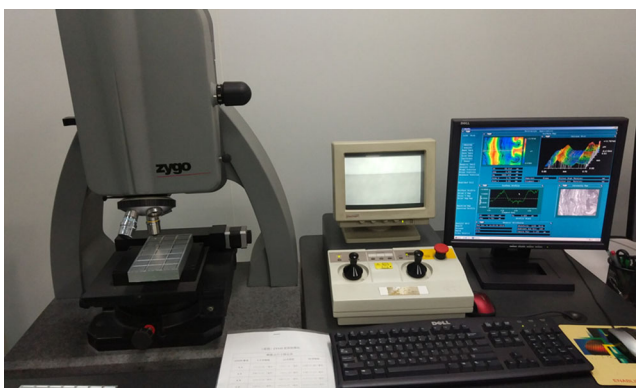

Fig. 12 Zygo NV5000 surface topography interferometer

Table 1 Selected cutting parameters for the study

Level	n/rmp	f_z/mm	w_p/mm	α/°	e/μm
1	3000	0.1	0.1	0	0
2	–	0.2	0.2	2	10
3	–	0.3	0.3	4	20
4	–	0.4	0.4	6	30
5	–	0.5	0.5	8	40
6	–	0.6	0.6	10	50
7	–	–	–	12	–
8	–	–	–	14	–
9	–	–	–	16	–
10	–	–	–	18	–
11	–	–	–	20	–

Table 2 Computation time of the simulation process

Examples	Number of the reference lines	Time (s)
Fig. 13b	243 × 363	19.56
Fig. 14b	243 × 363	20.39
Fig. 15b	483 × 363	41.78

5.2 Surface topography with different feed per tooth

Since the feed per tooth considers comprehensively the effect of the spindle speed and feedrate, only the topography and roughness of the machined surface with respective to feed per tooth is studied. The change of surface roughness with different feed per tooth is illustrated in Fig. 13a. It is seen that the roughness becomes large sharply as the feed per tooth increases. It shows the feed per tooth plays an important role for the surface quality. Especially, when the feed per tooth reaches within the visible range, for example, the feed per tooth is set 0.3 mm, the cutting action of the individual cutting edge may leave the obvious cutting cusp along the real trochoid path. The differences between the simulated and measured results may be a consequence of the material tearing from the workpiece since AL2024 is relatively soft and has large plastic deformation in the machining process. Besides, the built-up edge on the cutting edge is observed after cutting. This is also a reason why the difference occurs. In spite of this, the change trend of the simulated roughness is basically consistent with that of the experiment. Figure 13b, c shows, respectively, the simulated surface topography and the measured topography by the interferometer when the feed per tooth is 0.3 mm at the position enclosed by the red circle in Fig. 13a. By comparing Fig. 13b, c, it is seen that the proposed method can simulate effectively the topography of the machined surface. The computation time of the surface topography shown in Fig. 13b is 19.56 s, as shown in Table 2, which is accepted for the practical applications.

5.3 Surface topography with different tool orientation

To avoid the zero cutting speed when the tip of the ball-end cutter contacts the surface, the cutter usually declines an angle in the feed direction relative to the normal of the surface, i.e., the tilt angle, α, is kept a positive value, but the yaw angle, β, is usually set to be zero unless the global collision occurs. With the different tilt angles, the surface topography and roughness are simulated by the proposed method and measured using Zygo interferometer. Figure 14a gives the comparison of the simulated and measured roughness with different tilt angles. It is clearly seen that the change trend of the simulated and measured results is almost identical although there are some small deviations. With the increase of the tilt angle, the roughness reduces quickly, but after the tilt angle reaches a certain value, about 6° according to our experiment, the roughness is almost unchanged, but kept a stable value. Figure 14b, c gives the surface topography simulated by our method and measured by Zygo tester, respectively, when the tilt angle of cutter is 2° at the position enclosed by the red

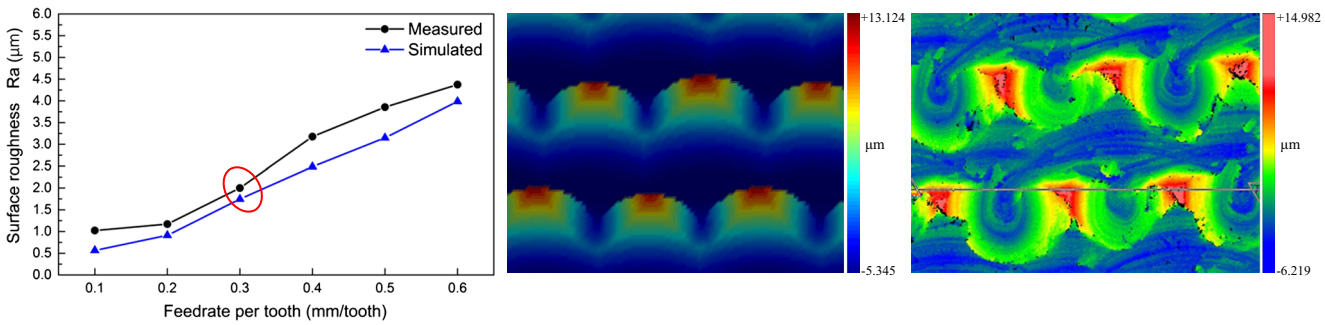

Fig. 13 Simulating and real milling with different feed per tooth when the path interval is 0.3 mm, the speed is 3000 rpm and tilt angle is 0°. **a** Change of surface roughness with feed per tooth. **b** Simulated surface topography. **c** Measured surface topography when feed per tooth is 0.3 mm

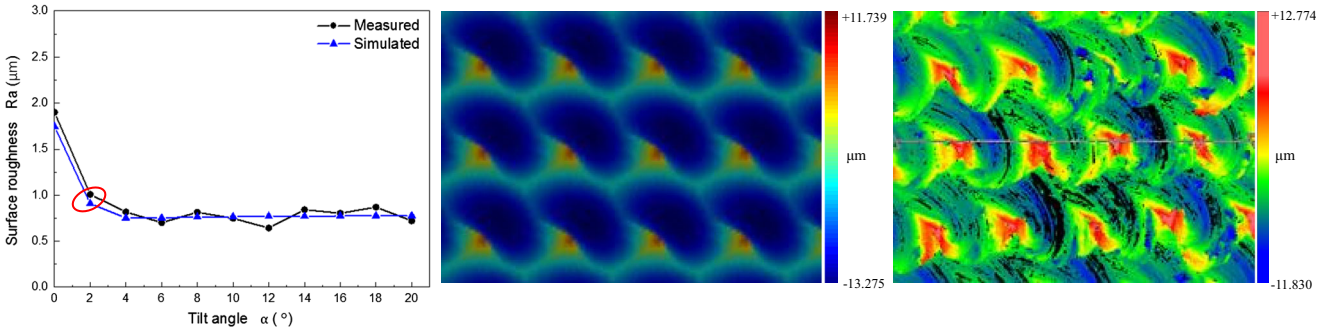

Fig. 14 Simulating and real milling with different tilt angles when the speed is 3000 rmp, the feed per tooth is 0.3 mm and the path interval is 0.3 mm. **a** Change of surface roughness with tilt angles. **b** Simulated surface topography. **c** Measured surface topography when tilt angle is 2°

circle in Fig. 14a. It is seen that the peak and valley of the simulated cusp reflects basically the changes of the real cutting cusp and shows good agreement with the measured results. The computation time of this example is 20.39 s, as shown in Table 2.

5.4 Surface topography with different path interval

Path interval is also a main factor which affects the surface topography and roughness. From Fig. 15a, it can be seen that either the simulated surface roughness or the measured one are both increased with the increase of the path interval and they show consistent change trend. Comparison of the simulated surface topography shown in Fig.15b and the measured one shown in Fig. 15c, when the feed per tooth is 0.3 mm/tooth, also shows that the cusp height change of the simulation results is corresponding basically to that of the actual experimental results either at the peak in red or the valley in blue of the cusp. This confirms that the proposed method can simulate well the milled surface. In addition, by comparing Fig. 13c and Fig. 15c, it is observed that, when the path interval is obviously larger than the feed per tooth, for example the path interval in Fig. 15 (c) is 0.6 mm and the feed per tooth is 0.3 mm/tooth, the cutting cusp in the path interval direction dominates in the surface topography and is almost continuous along the tool path. But, when the feed per tooth closes to the path interval, for example in Fig. 13c, the feed per tooth is 0.3 mm/tooth and the path interval is also 0.3 mm, the cutting cusp in the feed direction has larger influence on the surface quality. The computation time of this example is 41.78 s, as shown in Table 2.

5.5 Effect of cutter runout on topography and roughness

The effect of cutter runout is only studied by simulation, limited by our experiment conditions. From Fig. 16a, it is seen that the effect of cutter runout in five-axis machining on the surface roughness depends on the tilt angle of cutter. When the tilt angle is 0°, the surface roughness decreases slowly with the increase of the runout. But when the cutter inclines a tilt angle in the feed direction, the surface roughness become large sharply as the runout increases. After the runout reaches a certain value, about 30 μm in our experiments, the roughness is almost unchanged. In addition, Fig. 16b shows the simulated surface topography by the proposed method when using the same cutting parameters and cutter runout as given

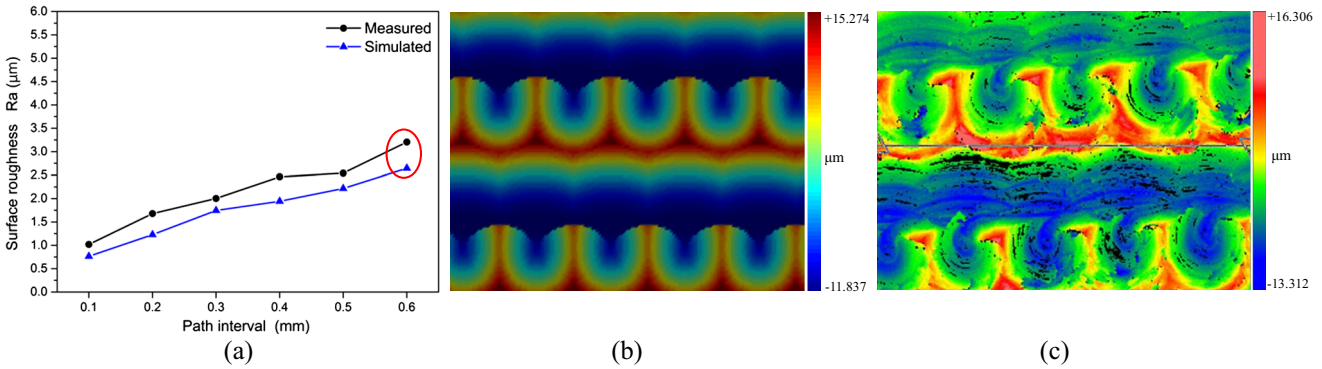

Fig. 15 Simulating and real milling with different path intervals when the feed per tooth is 0.3 mm, the speed is 3000 rpm, and the tilt angle is 0°. **a** Change of surface roughness with the path intervals. **b** Simulated surface topography. **c** Measured surface topography when the path interval is 0.6 mm

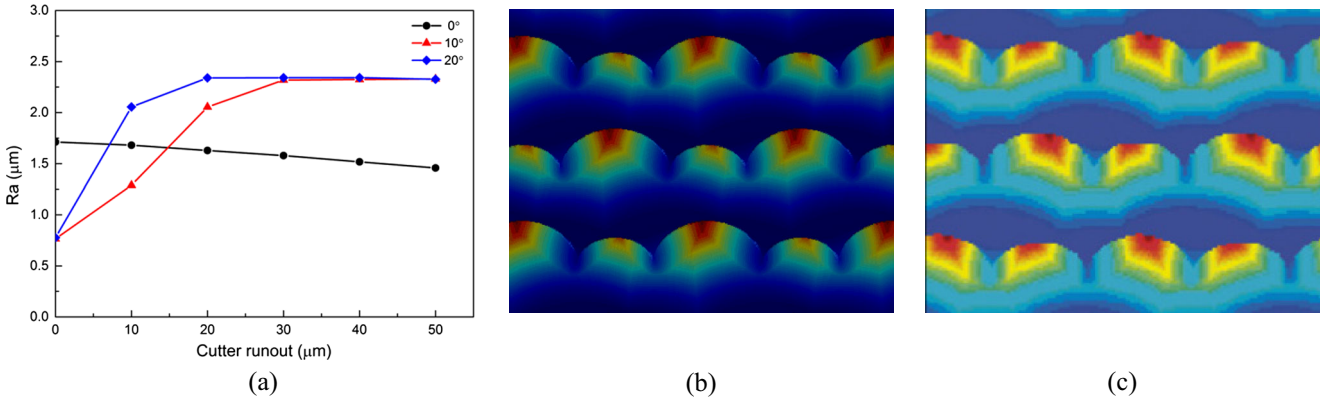

Fig. 16 Simulation with different tilt angle and cutter runout. **a** Change of surface roughness with cutter runout under different tilt angle. **b** Surface topography simulated by the proposed method when using the same parameter as Ref. [17], i.e., cutter runout e = 53 μm and tilt angle is 0°. **c** Surface topography simulated in Ref. [17]

by Arizmendi et al. in [17], and Fig. 16c is the simulated result by Arizmendi et al. By comparing Fig. 16b, c, it is seen that the simulated result by the proposed method shows good agreement with Arizmendi et al.'s. This demonstrates further the validity of our method. Analyzing and characterizing accurately the effect of the cutter runout on the topography of the surface by the actual cutting experiment will be our future work to be done.

6 Conclusions

This paper develops a swept surface approach to modeling the topography of the machined surface in the ball-end milling. In the study, the ball-end milling proceeds along a tool path is considered, from the view of kinematics, to be a process that the material is continuously removed by the swept surfaces of the cutting edges. Thus, the helix cutting edge of ball-end cutter used widely in CNC milling is first described accurately, and then its swept surface in WCS is modeled via a series of coordinate transformations, so that the cutting interaction of the cutter-workpiece can be more realistically described than before. On basis of this, a method based on interpolation is given to calculate accurately the cusp height of any point on the workpiece. It not only avoids the traditional numerical iteration of requiring good initial point to achieve the solution, but also eliminates the tolerance resulted from the discretizing parameter difference of cutting edge and workpiece in most methods. Although there are differences between the simulated and measured surface topography, the simulated results reflect well the variant characteristics of the surface topography, and the change trends of the simulated and measured surface roughness with various cutting parameters also show good agreement. This demonstrates the validity of the proposed method for simulating the surface topography in ball-end milling.

Acknowledgments This work is supported by the NSFC (Grant No. 51575086, 51525501) and the STBD (2016RD08).

References

1. Liu N, Wang SB, Zhang YF, Lu WF (2016) A novel approach to predicet surface roughness based on specific cutting energy consumption when slot milling Al-7075. Int J Mech Sci 118:13–20
2. Zhang C, Guo S, Zhang HY, Zhou LS (2013) Modeling and predicting for surface topography considering tool wear in milling process. Int J Adv Manuf Technol 68:2849–2860
3. Raja SB, Baskar N (2012) Application of particle swarm optimization technique for achieving desired milled surface roughness in minimum machining time. Exp Syst App 39(5):5982–5989
4. Chung YC, Park JW, Shin H, Choi BK (1998) Modeling the surface swept by a generalized cutter for NC verification. Comput Aided Des 30(8):584–587
5. Feng HS, Li HW (2002) Constant scallop-height tool path generation for three-axis sculptured surface machining. Comput Aided Des 34(9):647–654
6. Kim BH, Chu CN (1999) Texture prediction of milled surfaces using texture superposition method. Comput Aided Des 31(8): 485–494
7. Ryu SH, Choi DK, Chu CN (2006) Roughness and texture generation on end milled surfaces. Int J Mach Tools Manuf 46(3):404–412
8. Jung TS, Yang MY, Lee KJ (2005) A new approach to analysing machined surfaces by ball-end milling, part I: formulation of characteristic lines of cut remainder. Int J Adv Manuf Technol 25(9–10): 833–840
9. Jung TS, Yang MY, Lee KJ (2005) A new approach to analysing machined surfaces by ball-end milling, part II: roughness prediction and experimental verification. Int J Adv Manuf Technol 25(9–10): 841–849
10. Liu X, Soshi M, Sahasrabudhe A, Yamazaki K, Mori M (2006) A geometrical simulation system of ball end finish milling process and its application for the prediction of surface micro features. ASME Trans, J Manuf Sci Eng 128(1):74–85
11. Liu N, Loftus M, Whitten A (2005) Surface finish visualisation in high speed, ball nose milling applications. Int J Mach Tools Manuf 45(10):1152–1161

12. Antoniadis A, Savakis C, Bilalis N, Balouktsis A (2003) Prediction of surface topomorphy and roughness in ball-end milling. Int J Adv Manuf Technol 21(12):965–971
13. Buj-Corral I, Vivancos-Calvet J, Domínguez-Fernández A (2012) Surface topography in ball-end milling processes as a function of feed per tooth and radial depth of cut. Int J Mach Tools Manuf 53(1):151–159
14. Bouzakis KD, Aichouh P, Efstathiou K (2003) Determination of the chip geometry, cutting force and roughness in free form surfaces finishing milling, with ball end tools. Int J Mach Tools Manuf 43(5):499–514
15. Omar OEEK, El-Wardany T, Ng E, Elbestawi MA (2007) An improved cutting force and surface topography prediction model in end milling. Int J Mach Tools Manuf 47(7):1263–1275
16. Zhang C, Zhang H, Li Y, Zhou L (2015) Modeling and on-line simulation of surface topography considering tool wear in multi-axis milling process. Int J Adv Manuf Technol 77(1–4):735–749
17. Arizmendi M, Fernández J, de Lacalle LL, Lamikiz A, Gil A, Sánchez JA, Campa FJ, Veiga F (2008) Model development for the prediction of surface topography generated by ball-end mills taking into account the tool parallel axis offset. Experimental validation. CIRP Annals-Manuf Technol 57(1):101–104
18. Chen JS, Huang YK, Chen MS (2005) A study of the surface scallop generating mechanism in the ball-end milling process. Int J Mach Tools Manuf 45(9):1077–1084
19. Zhang WH, Tan G, Wan M, Gao T, Bassir DH (2008) A new algorithm for the numerical simulation of machined surface topography in multiaxis ball-end milling. ASME Trans, J Manuf Sci Eng 130(1):011003
20. Quinsat Y, Sabourin L, Lartigue C (2008) Surface topography in ball end milling process: description of a 3D surface roughness parameter. J Mater Process Technol 195(1):135–143
21. Lavernhe S, Quinsat Y, Lartigue C (2010) Model for the prediction of 3D surface topography in 5-axis milling. Int J Adv Manuf Technol 51(9–12):915–924
22. Quinsat Y, Lavernhe S, Lartigue C (2011) Characterization of 3D surface topography in 5-axis milling. Wear 271(3):590–595
23. Mizugaki Y, Hao M, Kikkawa K, Nakagawa T (2001) Geometric generating mechanism of machined surface by ball-nosed end milling. CIRP Annals-Manuf Technol 50(1):69–72
24. Li ZL, Zhu LM (2014) Envelope surface modeling and tool path optimization for five-axis flank milling considering cutter runout. ASME Trans, J Manuf Sci Eng 136:41021
25. Schneider PJ, Eberly DH (2005) Geometric tool for computer graphics (in Chinese and translated by Zhou CF). Publishing House of Electronics Industry, Beijing